Received November 2002
Revised April 2003
Accepted April 2003

# Microscopic and macroscopic approach for natural convection in enclosures filled with fluid saturated porous medium

N. Massarotti
*Dipartimento di Meccanica, Strutture, Ambiente e Territorio (DIMSAT), Università degli Studi di Cassino, Cassino, Italy*

P. Nithiarasu
*Civil and Computational Engineering Center, School of Engineering, University of Wales Swansea, Swansea, UK*

A. Carotenuto
*Dipartimento di Meccanica, Strutture, Ambiente e Territorio (DIMSAT), Università degli Studi di Cassino, Cassino, Italy*

***Keywords*** *Porous materials, Compressible flow, Convection*

***Abstract*** *In this paper, microscopic and macroscopic approaches to the solution of natural convection in enclosures filled with fluid saturated porous media are investigated. At the microscopic level, the porous medium is represented by different assemblies of cylinders and the Navier-Stokes equations are assumed to govern the flow. To represent the flow in a macroscopic porous medium approach, the generalised flow model is employed. The characteristic based split scheme is used to solve the conservation equations of both approaches. In addition to the comparison between microscopic and macroscopic approaches of fluid saturated porous enclosures, cavities with interface between fluid saturated porous medium and single phase fluid are also investigated.*

## 1. Introduction

Flow through porous media is a well recognised research area in which researchers are still trying to understand some of the modelling aspects. When the flow in porous media is combined with heat and mass transfer, dispersion and turbulence, significant modelling difficulties are encountered. Modern day research into porous medium flow employs the fundamental principles for the solution of complicated applied problems where some kind of porous medium, either natural or man made, is involved.

This research is partially funded by EPSRC through grant GR/R29321/01.

International Journal of Numerical Methods for Heat & Fluid Flow
Vol. 13 No. 7, 2003
pp. 862-886

0961-5539
DOI 10.1108/09615530310502073

The models available for flow in the porous media are generally based on the experimental observations and averaging. Such a *macroscopic* approach is traditionally used in the analysis of flow through soils, insulation and packed beds. This macroscopic approach gives no details at the particle level. On the other hand, the Navier-Stokes equations can be used to solve many porous medium problems at a *microscopic* level. However, such an approach may become very difficult and expensive, although it gives minute details of flow structure at particle level. A proper understanding of the relations between these two approaches can lead to cost reductions in many CFD calculations. The main objective of the present work is to investigate the relations between the two approaches, when these are used to solve natural convection flow problems through saturated porous media.

Flow modelling in fluid saturated porous media started with the simple, phenomenological relation proposed by Darcy (1856) in the 19th century in the context of flow through soils. Later, two major extensions to the Darcy model have made the subject interesting and widely useful in many engineering disciplines including chemical, mechanical and civil engineering problems. The first extension was due to Forchheimer (1901) and his modification accounted for moderate and high Reynolds number effects through the addition of a non-linear term to the Darcy's equation. However, such a modification was still not able to predict flow through high porosity and confined media. In 1947, Brinkman introduced an extension to the Darcy model which included a second order viscous term with an equivalent viscosity for the porous medium (Brinkmann, 1947). This latter modification allows the use of no-slip conditions on confining walls and gives accurate results at higher porosity values (Gilver and Altobelli, 1994; Tong and Subramanian, 1986).

With the advent of computational power, flow modelling in porous media received a significant boost and the model known as *Generalised model* was introduced. The first attempt to construct such a model was made by Whitaker (1961) and later using the volume averaging principles by Hsu and Cheng (1990) and Vafai and Tien (1981). Recently, a control volume principle was introduced by (Nithiarasu *et al.*, 1997) to derive such a generalised model. In many ways, the generalised model is useful as it is very similar to that of the Navier-Stokes equations. It was proved to approach the single phase flow when the porosity approaches unity (Nithiarasu *et al.*, 1997), and it was also proved that the porosity has a very significant role at higher permeability values.

The two extensions introduced after Darcy model are generally known as *non-Darcy models* and are used to solve flow with many limitations. However, the generalised porous medium model can eliminate those limitations (Nithiarasu *et al.*, 1997), and is therefore used in this work.

Although there are many numerical procedures available in the literature, the velocity correction based procedure introduced by Nithiarasu *et al.* (1996) for porous medium flows has many advantages over other methods. Many

early researchers ignored the transient effects, but several porous medium flows require transient analysis. As the velocity correction based method is a time stepping scheme, treating the transient flow problems is natural. The computations using the finite element methods were proved efficient as the velocity correction procedure has no incompressibility Babuska-Brezzi (BB) restrictions. Also, implementation of different schemes such as semi-implicit schemes (Nithiarasu and Ravindran, 1998; Nithiarasu *et al.*, 2000) quasi-implicit schemes (Nithiarasu *et al.*, 1996) and fully implicit schemes is possible. Applications of such procedures include underground water pollution (Nithiarasu *et al.*, 1998a, b; Nithiarasu, 1999) and porous fluid interfaces (Massarotti *et al.*, 2000; Nithiarasu *et al.*, 2002).

Many areas of flow through porous media are well understood in the fundamental sense. However, still not much has been done in the context of complicated man-made industrial problems such as flow through turbo-machines, flow due to cooling of electronic equipments, flow and heat transfer during heating and cooling of storage and domestic buildings. The complexity of such applied problems arise due to the structure of the geometry involved. In many cases, a computational study of the minute details can be extremely time consuming and analysis relies mainly upon experimental trials. However, the averaged porous medium approach can be used in these applications to estimate some key design parameters such as rate of heat loss, drag, pressure drop etc. Such a porous medium approximation is used in applications such as alloy solidification (Prescott and Incropera, 1994), turbo machines (Maji and Biswas, 1999) and in electronic cooling arrangements (Fu and Chen, 2002; Heindel *et al.*, 1996; Zhao and Lu, 2002). These studies have used the porous medium approach in a rather empirical way by some kind of simple addition and thus their accuracy is still not well established. Several questions, such as what are the limitations of these additions and how close the results are to reality, are still unanswered.

In some common real life problems, such as thermal insulation problems, geothermal wells, and porous media drying applications, an interface exists between the porous medium and the free fluid. A set of proper matching conditions is needed at the interface, irrespective of the model used to describe the porous medium flow. For the generalised model, an appropriate value of the effective viscosity of the porous medium can provide such conditions. However, determination of this parameter is still not an easy task, and therefore its value is still unknown for several applications (Gartling *et al.*, 1996; Gilver and Altobelli, 1994; Kladias and Prasad, 1991; Koplik *et al.*, 1983; Marty *et al.*, 1994). Furthermore, most of the work for the determination of the effective viscosity and other macroscopic parameters, such as the permeability, has been carried out for forced convection problems (Gupte and Advani, 1997; Kaviany, 1991; Lee and Yang, 1997; Martys *et al.*, 1994, Nakayama and Kuwahara, 2000; Wang, 1999). In forced flow, the influence of the effective viscosity has been

shown to be not very strong (Alazmi and Vafai, 2001). However, in the case of natural convection, this influence may become relevant especially for media of higher porosity (Massarotti, 2001; Massarotti *et al.*, 2000). In fact, in this type of problems the fluid is driven by buoyancy forces due to temperature gradients, therefore the pressure losses do not play such a relevant role in the fluid motion, as in the case of forced convection. Despite the large number of investigations carried out in the last decades Oosthuizen, 2000), there is still a clear lack of knowledge in the field of natural convection in the porous medium, and the comparison between the microscopic and macroscopic approaches to the solution of this type of problems with interface between the porous medium and the free fluid.

From the above discussion, it is obvious that a comparative study of microscopic and macroscopic approach can lead to further understanding of the topic and solve some of the mentioned problems. In this paper, we present several cases of natural convection in porous media using the microscopic and macroscopic approaches. In the following section, the governing equations and non-dimensional scales used are discussed. In Section 3, the numerical scheme is briefly described followed by the results in Section 4. Finally, conclusions from the present study are given in Section 5.

## 2. The governing equations

The generalised model for the description of flow through the saturated porous media of a single phase incompressible fluid consists of a set of conservation equations. Assuming local thermal equilibrium and uniform properties of the porous medium, the governing equations in the non-dimensional form can be written as:

$$\frac{\partial \mathbf{W}}{\partial t} + \frac{\partial \mathbf{F}_j}{\partial x_j} - \frac{\partial \mathbf{G}_j}{\partial x_j} = \mathbf{S} \tag{1}$$

with

$$\mathbf{W} = \begin{pmatrix} 0 \\ \frac{1}{\varepsilon} u_1 \\ \frac{1}{\varepsilon} u_2 \\ R_c T \end{pmatrix}, \qquad \mathbf{F}_j = \begin{pmatrix} u_j \\ \frac{1}{\varepsilon^2} u_1 u_j + p\delta_{1j} \\ \frac{1}{\varepsilon^2} u_2 u_j + p\delta_{2j} \\ R_c T u_j \end{pmatrix}, \qquad \mathbf{G}_j = \begin{pmatrix} 0 \\ \frac{1}{\varepsilon} \tau_{1j} \\ \frac{1}{\varepsilon} \tau_{2j} \\ R_k \frac{\partial T}{\partial x_j} \end{pmatrix},$$

$$\mathbf{S} = \mathbf{S}_A + \mathbf{S}_B = \begin{pmatrix} 0 \\ -Pu_1 \\ -Pu_2 \\ 0 \end{pmatrix} + \begin{pmatrix} 0 \\ 0 \\ \mathrm{RaPr}T \\ 0 \end{pmatrix}$$

in which the coefficient $P$ is defined as

$$P = \frac{\mathrm{Pr}}{\mathrm{Da}} + \frac{1.75}{\sqrt{150}} \frac{\sqrt{u_k u_k}}{\sqrt{\mathrm{Da}}} \frac{1}{\varepsilon^{3/2}} \tag{2}$$

In the above equation, the well known Ergun relation (Ergun, 1952) for the permeability has been employed in order to consider both viscous and inertial energy losses in the porous medium. The intrinsic permeability of the porous medium is calculated as:

$$\kappa = \frac{d_s^2 \varepsilon^3}{150(1-\varepsilon)^2} \tag{3}$$

in which $d_s$ is the diameter of the solid particle and $\varepsilon$ the porosity of the medium, defined as the volume fraction occupied by the fluid in a saturated porous medium, $\varepsilon = V_f / V_p$. $V_f$ is the volume of the matrix left to the fluid and $V_p$ is the total volume occupied by the porous medium, which is the sum of that occupied by the solid matrix and $V_f$.

The non-dimensional form of deviatoric stress is defined by

$$\tau_{ij} = R_v \mathrm{Pr} \left( \frac{\partial u_i}{\partial x_j} + \frac{\partial u_j}{\partial x_i} - \frac{2}{3} \frac{\partial u_k}{\partial x_k} \delta_{ij} \right) \tag{4}$$

The force of gravity is considered to act along the $x_2$ direction as is evident by the inclusion of the buoyancy term in the $x_2$ component of momentum equation.

In the non-dimensional form of the generalised model equations (equation (1)), the following scales and parameters have been employed:

$$x_j = \frac{x_j^*}{L}, \qquad u_j = \frac{u_j^*}{\alpha_f / L}, \qquad p = \frac{p^*}{(\rho \alpha^2)_f / L^2}, \qquad t = \frac{t^*}{L^2 / \alpha_f},$$

$$T = \frac{T^* - T_c^*}{T_h^* - T_c^*}, \qquad R_c = \frac{(1-\varepsilon)(\rho c_p)_s + \varepsilon (\rho c_p)_f}{(\rho c_p)_f}, \qquad R_v = \frac{\mu_e}{\mu_f}, \tag{5}$$

$$R_k = \frac{k_e}{k_f}, \qquad \mathrm{Pr} = \frac{\nu_f}{\alpha_f}, \qquad \mathrm{Ra} = \frac{g \beta \Delta T L^3}{(\nu \alpha)_f}, \qquad \mathrm{Da} = \frac{\kappa}{L^2}$$

where asterisk is used for the dimensional variables, subscripts f and s refer to the fluid and the solid properties, respectively, $\alpha$ is the thermal diffusivity, $\beta$ the coefficient of thermal expansion, $\mu$ and $\nu$ the dynamic and kinematic viscosities, respectively, $\rho$ the density, $c_p$ the specific heat at constant pressure, $x_j^*$ are the position vector components, $t^*$ is the time, $u_j^*$ are the Darcy velocity components, $p^*$ is the pressure and $T^*$ the temperature over the representative elementary volume (REV), $g$ represents the magnitude of the gravitational acceleration, $T_h^*$ and $T_c^*$ are, respectively, the hot and cold wall temperatures, and $L$ is the characteristic length of the problem considered. Non-dimensional

parameters include $R_c$ the average volumetric heat capacity ratio, which has been assumed to be constant in this work, $R_v$ the ratio between the effective viscosity of the porous medium and the fluid viscosity, and $R_k$ the ratio between the effective conductivity of the porous medium (evaluated considering stagnant saturating fluid) and the fluid thermal conductivity. The parameters Pr, Ra and Da represent the Prandtl, Rayleigh and Darcy numbers, respectively.

The generalised model equations (equation (1)) discussed above reduce to the Navier Stokes equations when the solid matrix in the porous medium disappears, i.e. when $\varepsilon \rightarrow 1$ and $\mathrm{Da} \rightarrow \infty$. Therefore, the same set of equations can be used for the microscopic solution of the problem using the same numerical algorithm, described in the following sections, by assuming that the porosity is 1 and the coefficient $P$ is 0. Furthermore, the procedure can be used for the solution of porous medium – free fluid interface problems, using a single domain approach and changing the property of the medium in the computational domain appropriately.

## 3. Solution procedure

In this section, the characteristic based split (CBS) procedure employed for the solution of porous medium equations is described. As mentioned, the velocity and temperature fields in the single phase free fluid can also be obtained using the same procedure, by setting properly the values of $\varepsilon$ and $P$.

### *3.1 Temporal discretization*

The momentum equation introduced in the generalised model is a typical convection-diffusion equation and can therefore be discretized in time using the characteristic process. In particular, time discrete momentum equation in the semi-implicit form of the scheme can be written as (Massarotti *et al.*, 2001; Nithiarasu *et al.*, 2002; Zienkiewicz and Taylor, 2000):

$$u_i^{n+1} - u_i^n + \varepsilon \Delta t P u_i^{n+1} = \varepsilon \Delta t \left[ -\frac{1}{\varepsilon^2} \frac{\partial}{\partial x_j}(u_i u_j)^n - \frac{\partial p^{n+\theta_2}}{\partial x_i} + \frac{\partial \tau_{ij}^n}{\partial x_j} + \mathrm{RaPr} T^n g_i \right] + \varepsilon \frac{\Delta t^2}{2} \left[ u_k \frac{\partial}{\partial x_k} \left( \frac{1}{\varepsilon^2} \frac{\partial}{\partial x_j}(u_i u_j) + \frac{\partial p}{\partial x_i} - \mathrm{RaPr} T g_i \right) \right]^n \quad (6)$$

where the pressure term is not treated explicitly, but is evaluated at a time $t^n + \theta_2 \Delta t$ and is given by

$$\frac{\partial p^{n+\theta_2}}{\partial x_i} = \theta_2 \frac{\partial p^{n+1}}{\partial x_i} + (1 - \theta_2) \frac{\partial p^n}{\partial x_i} \quad (7)$$

Note that in this study it was assumed that $\theta_2 = 1$.

For the solution of these equations, the CBS algorithm uses a fractional step with a split. In the first step, a new variable $u_i^*$ is defined such that

$$u_i^* - u_i^n + \varepsilon \Delta t P u_i^* = \varepsilon \Delta t \left[ -\frac{1}{\varepsilon^2} \frac{\partial}{\partial x_j}(u_i u_j) + \frac{\partial \tau_{ij}}{\partial x_j} + \mathrm{RaPr} T g_i \right]^n + \varepsilon \frac{\Delta t^2}{2} \left[ u_k \frac{\partial}{\partial x_k} \left( \frac{1}{\varepsilon^2} \frac{\partial}{\partial x_j}(u_i u_j) - \mathrm{RaPr} T g_i \right) \right]^n \tag{8}$$

This represents the first part of the split and is explicit. The corrected velocities can be determined, once the pressure is known, using the equation

$$u_i^{n+1} - u_i^* + \varepsilon \Delta t P \left( u_i^{n+1} - u_i^* \right) = \varepsilon \Delta t \left[ -\frac{\partial p^{n+\theta_2}}{\partial x_i} + \frac{\Delta t}{2} u_k \frac{\partial}{\partial x_k} \left( \frac{\partial p^n}{\partial x_i} \right) \right] \tag{9}$$

The solution of this equation is actually the third step in the algorithm. The second step is the determination of the pressure, from the following Poisson type of equation:

$$\theta_2 \frac{\partial^2 p^{n+1}}{\partial x_i \partial x_i} = \frac{\partial}{\partial x_i} \left[ \frac{u_i^*}{\varepsilon \Delta t} + P u_i^* \right] - (1 - \theta_2) \frac{\partial^2 p^n}{\partial x_i \partial x_i} \tag{10}$$

The fourth step of the algorithm involves the calculation of the temperature field using the energy conservation equation. For incompressible flow, characteristic time discretization of this equation gives

$$T^{n+1} - T^n = \frac{\Delta t}{R_c} \left[ -\frac{\partial}{\partial x_j}(T u_j) + \frac{\partial}{\partial x_j} \left( R_k \frac{\partial T}{\partial x_j} \right) \right]^n + \frac{\Delta t^2}{2} \left[ u_k \frac{\partial}{\partial x_k} \left( \frac{\partial}{\partial x_j}(T u_j) \right) \right]^n \tag{11}$$

The second order terms, in equations (6) and (9) multiplied by $\Delta t^2$, provide convective stabilization.

*3.2 Spatial discretization*

The above equations are then discretized in space using the standard Galerkin finite element procedure. The computational domain is therefore subdivided into a triangular mesh of finite elements. Within an element, each variable is approximated by a linear function, which can be expressed in terms of the variable value at each of the three nodes of the element:

$$\phi = \sum_{n=1}^{3} N_n \bar{\phi}_n \tag{12}$$

where $N_n$ is the shape function at node $n$ and $\bar{\phi}_n$ is the value of the generic variable $\phi$ at node $n$.

The equations obtained substituting the approximated function in equations (6)-(9) are then weighted using the same shape functions, $N_n$, and integrated over the whole domain. The resulting system of ordinary algebraic equations can be written as follows.

*Step 1.* Intermediate velocity calculation

$$\mathbf{M}\left(u_i^* + \varepsilon\Delta t P u_i^*\right) = \mathbf{M}u_i + \varepsilon\Delta t\left[\frac{1}{\varepsilon^2}\mathbf{C}u_i + \mathbf{K}_\tau + \mathrm{RaPr}\mathbf{M}Tg_i\right]^n + \frac{\varepsilon\Delta t^2}{2}\left[\mathbf{K}_\mathrm{u}u_i - \mathrm{RaPr}\mathbf{Q}_\mathrm{u}\right]^n + \mathrm{bt} \tag{13}$$

*Step 2.* Pressure calculation

$$\theta_2\mathbf{K}p^{n+1} = \mathbf{D}\left(\frac{1}{\varepsilon\Delta t}u_i^* + Pu_i^*\right) - (1-\theta_2)\mathbf{K}p^n \tag{14}$$

*Step 3.* Velocity correction

$$\mathbf{M}\left(u_i^{n+1} + \varepsilon\Delta t P u_i^{n+1}\right) = \mathbf{M}\left(u_i^* + \varepsilon\Delta t P u_i^*\right) - \varepsilon\Delta t\mathbf{D}p^{n+1} \tag{15}$$

*Step 4.* Temperature calculation

$$\mathbf{M}\mathbf{T}^{n+1} = \mathbf{M}\mathbf{T}^n - \frac{\Delta t}{R_\mathrm{c}}\mathbf{C}\mathbf{T}^n + \Delta t\frac{R_\mathrm{k}}{R_\mathrm{c}}\mathbf{K}\mathbf{T}^n + \frac{\Delta t^2}{2}(\mathbf{K}_\mathrm{u}\mathbf{T})^n + \mathrm{bt} \tag{16}$$

where

$$\mathbf{M} = \int_\Omega \mathbf{N}^\mathrm{T}\mathbf{N}\,\mathrm{d}\Omega \quad \mathbf{C} = \int_\Omega \mathbf{N}^\mathrm{T}(\nabla(\mathrm{u}\mathbf{N}))\,\mathrm{d}\Omega \quad \mathbf{D} = \int_\Omega (\nabla\mathbf{N}^\mathrm{T})^\mathrm{T}\mathbf{N}\,\mathrm{d}\Omega$$

$$\mathbf{Q}_\mathrm{T} = \int_\Omega (\nabla^\mathrm{T}(\mathrm{u}\mathbf{N}))^\mathrm{T}\mathbf{T}g_i\,\mathrm{d}\Omega \quad \mathbf{K} = \int_\Omega (\nabla\mathbf{N}^\mathrm{T})^\mathrm{T}\nabla\mathbf{N}\,\mathrm{d}\Omega \tag{17}$$

$$\mathbf{K}_\mathrm{u} = \int_\Omega (\nabla^\mathrm{T}(\mathrm{u}\mathbf{N}))^\mathrm{T}(\nabla^\mathrm{T}(\mathrm{u}\mathbf{N}))\,\mathrm{d}\Omega \quad \mathbf{K}_\tau = \int_\Omega \mathbf{N}^\mathrm{T}(\nabla\tau)\,\mathrm{d}\Omega$$

Here $\Omega$ corresponds to the entire computational domain and bt represents the boundary terms that are derived from the integration by parts of the second order derivatives in the partial differential equations. In equations (11)-(14), $\mathbf{M}$ is the mass matrix which is lumped in this work in order to simplify the calculations. The interested reader should refer to other publications which gives a complete description of this method (Massarotti *et al.*, 2001; Nithiarasu *et al.*, 2002; Zienkiewicz and Taylor, 2000).

Equations (11)-(14) can be used for the solution of incompressible natural convective porous medium flow and for the single phase fluid flows with appropriate changes in the porosity and permeability values. It is also possible to handle porous medium free fluid interface problems using a single domain approach (Beckermann *et al.*, 1987; Song and Viskanta, 1994), by changing the properties of the medium properly, as it will be seen in the next section. The following porosity limits are used for the porous medium and single-phase fluid domains:

$$\begin{matrix} \varepsilon = 1 \\ \mathrm{Da} \rightarrow \infty \end{matrix} \Rightarrow \text{free} \quad \text{fluid} \qquad \begin{matrix} \varepsilon < 1 \\ \mathrm{Da} = \text{finite} \end{matrix} \Rightarrow \text{porous} \ \ \text{medium} \tag{18}$$

The steady-state results of equations (11)-(14) are presented in Section 4. The solution is obtained by reducing the maximum difference in velocity and temperature values between the consecutive time steps to a fixed minimum tolerance. In the present study this tolerance is taken equal to $10^{-6}$.

## 4. Results

In this section, the numerical results obtained using the microscopic and the macroscopic approaches are presented. The CBS algorithm has proved to produce accurate results for all type of fluid dynamic problems, both isothermal (Zienkiewicz and Taylor, 2000), and non-isothermal (Massarotti *et al.*, 1998, 2001). In the following subsection, the present procedure is validated considering a simple square cavity filled with a porous medium. The flow in the cavity is due to the buoyancy force produced by the difference in temperature imposed on the vertical walls of the cavity. Later, the same approach is used to study the interface problems between a saturated porous medium and a free fluid.

### *4.1 Natural convection in a saturated porous medium*

The first problem considered is a comparative study between the microscopic and the macroscopic approaches for the solution of natural convective flow in a fluid saturated porous medium. The computational domains used are presented in Figure 1. Figure 1(a) depicts the microscopic porous medium in which the solid particles are assumed to be circular in shape and arranged in line, staggered or placed arbitrarily. The number of cylinders used is different in each of the arrangements considered in order to construct problems with different permeability and porosity values. The macroscopic domain, shown in Figure 1(b), has the same scales as the microscopic medium. The values of the parameters $\varepsilon$ and $\kappa$ for this medium are obtained from their definitions given in the previous section and are presented in Table I. The minimum value of the porosity considered is just greater than the value of 0.6 which is happened to be the limit for the applicability of the Brinkman extension of the Darcy's law (Brinkmann, 1947, 1948).

The boundary conditions assumed for both approaches, presented in Figure 1, are obviously the same. All walls have no-slip velocity conditions, the horizontal walls are considered to be thermally insulated, while the vertical walls are kept at different temperatures. Furthermore, the solid particles considered in the microscopic domain are assumed to be adiabatic, in order to justify the assumption of local thermal equilibrium made for the macroscopic approach.

It is important to discuss here one of the scales employed for non-dimensionalisation. It should be noted that the length scale $L$ used in this paper is the diameter of the cylindrical solid particles. All the values of the Rayleigh numbers calculated in this paper are based on the length scale $L$ and fall within the range of 10-$10^5$. However, re-scaling this range based on the domain height leads to a Rayleigh number range of $10^3$-$10^8$. The same consideration apply to all other parameters that include $L$, as for example the Darcy number. The fluid considered to saturate the cavities is air, and a Prandtl number of 0.72 is assumed for it.

A mesh sensitivity analysis was carried out independently for the microscopic and macroscopic approaches. The optimal number of elements was determined when the solution, in terms of the main quantities of interest, such as average Nusselt number velocity etc., was nearly independent of the number of nodes considered. Figure 2 shows the final meshes employed for the two approaches to the porous cavity problem. The first three meshes shown in

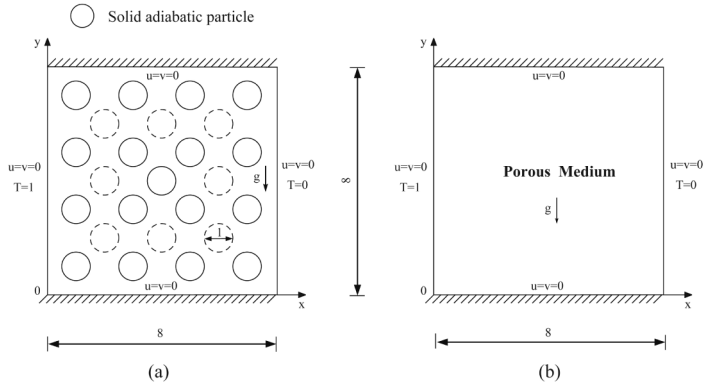


**Figure 1.**
Computational domain and boundary conditions used for the macroscopic (right) and the microscopic (left) approaches

| Microscopic | | Macroscopic | |
|---|---|---|---|
| Number of cylinders | Arrangement | $\varepsilon$ | $\kappa$ |
| 16 | In line | 0.804 | $8.98 \times 10^{-2}$ |
| 25 | Staggered | 0.693 | $2.36 \times 10^{-2}$ |
| 32 | Arbitrary | 0.607 | $9.68 \times 10^{-3}$ |

**Table I.**
Microscopic configurations considered and related macroscopic parameters

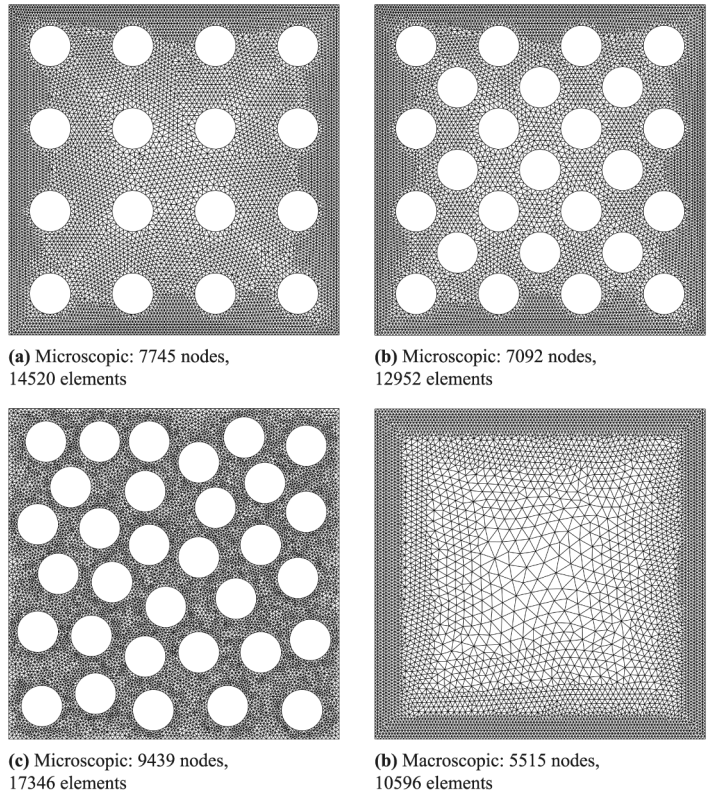


**Figure 2.**
Finite element meshes used for the microscopic and macroscopic approaches. (a) In-line, (b) staggered, (c) arbitrary arrangements and (d) macroscopic medium

Figure 2 have been used to solve the natural convection microscopically. Figure 2(a) represents the mesh used for the first case with 16 cylinders arranged in line, Figure 2(b) is the mesh for the case with 25 staggered cylinders, and Figure 2(c) presents the mesh for the 32 arbitrarily placed cylinders. Finally, in the same figure the mesh used for the macroscopic approach is also presented (Figure 2(d)).

The results obtained using these meshes are presented in Figures 3-6 in terms of the streamlines and isotherms. Figure 3 shows the isotherms (top) and streamlines (bottom) for the first case considered ($\varepsilon = 0.804$, $\mathrm{Da} = 8.98 \times 10^{-2}$), obtained using the microscopic (left) and macroscopic (right) approaches at a Rayleigh number of $10^4$. It can be seen from the picture that similarity exists between the isotherms and the streamlines obtained using the microscopic and macroscopic approaches. As expected the flow pattern of the microscopic approach contain several small vortices due to the complicated structure of the medium. However, the major vortex covering the two central rows of cylinders (Figure 3(c)) is very similar to the vortex structure of the macroscopic approach (Figure 3(d)). Figure 4 shows the isotherms and

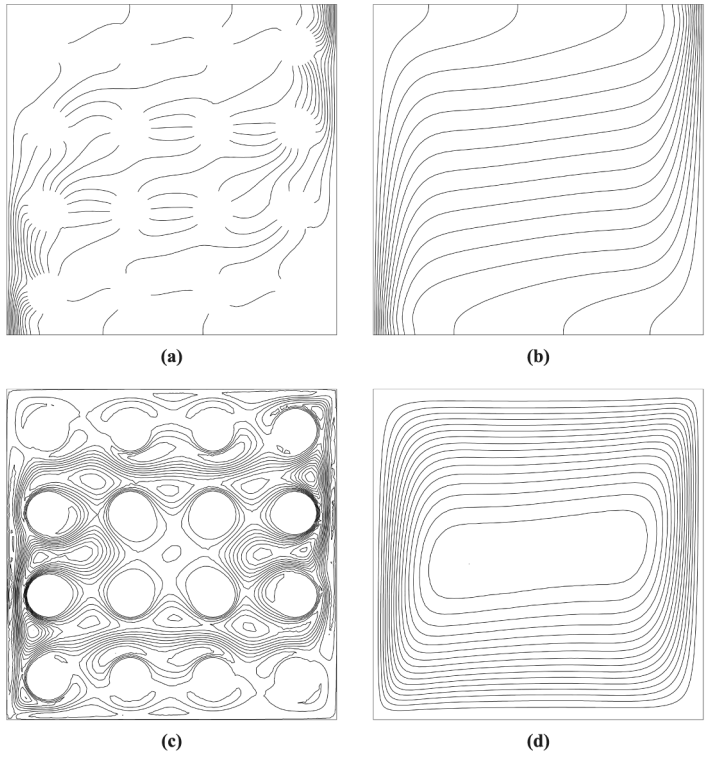


**Figure 3.**
Macroscopic (right) and microscopic (left) solutions. Isotherms (a, b) and streamlines (c, d) at $Ra = 10^4$ for the first case considered (macroscopic parameters: $\varepsilon = 0.804$, $Da = 8.98 \times 10^{-2}$)

the streamlines for the second case with staggered cylinder arrangement. The calculated Darcy number of this case is $2.36 \times 10^{-2}$ and the porosity is 0.693. The Rayleigh number value is the same as the previous case and equal to $10^4$. Compared to the previous case the Darcy number and the porosity are lower in the present case. The isotherm patterns of the microscopic and macroscopic approaches look very similar as shown in Figures 4(a) and (b). The flow patterns are also similar, but the microscopic approach gives the details of vortices close to the cylindrical particles. It should be noted that, compared to the previous case (Figure 3(c)-(d)) the eye of the vortex in the macroscopic approach is rotated towards the top right and bottom left corners of the cavity (Figure 4(d)). This behaviour is also represented by the results of the microscopic approach (Figure 4(c)). All the similarities between the microscopic and the macroscopic approaches show that the generalised macroscopic flow model is effective in predicting accurate results. For the two cases discussed in the previous paragraphs, the grain arrangement in the microscopic medium followed certain pattern. However, in the next case, the grains are placed arbitrarily in the medium, as shown in Figure 5. The Darcy number and porosity values calculated are the lowest of all the cases considered and equal

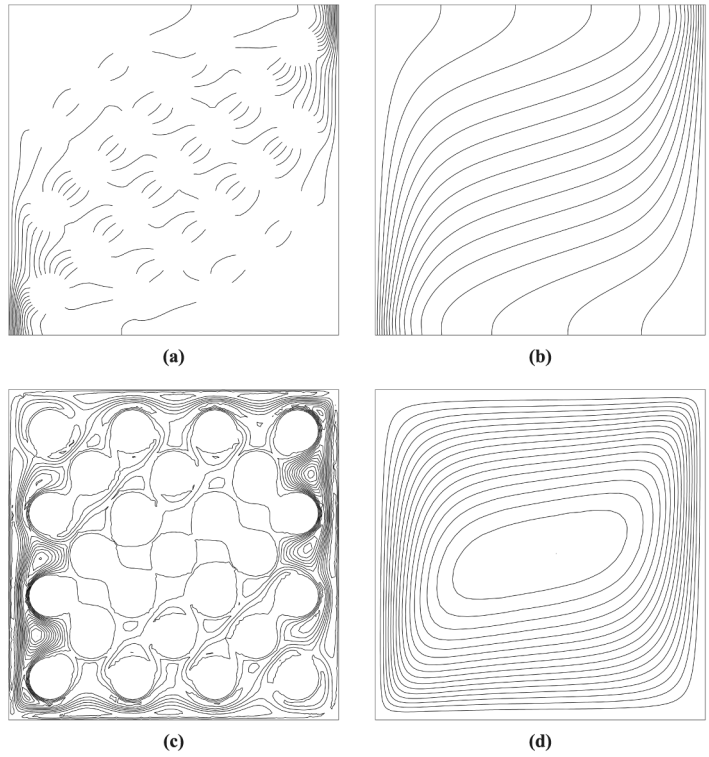


**Figure 4.**
Macroscopic (right) and microscopic (left) solutions. Isotherms (a, b) and streamlines (c, d) at $Ra = 10^4$ for the second case considered (macroscopic parameters: $\varepsilon = 0.693$, $Da = 2.36 \times 10^{-2}$)

to $9.68 \times 10^{-3}$ and 0.607, respectively. As in the previous cases, the isothermal and flow patterns of the microscopic and macroscopic approaches are very similar. However, the microscopic pattern is unsymmetric due to the arbitrary arrangement of the cylinders. It is obvious that the macroscopic approach for this case can only produce symmetric patterns with uniform properties and Darcy number. It may be possible to predict the unsymmetric patterns if a variation in porosity and Darcy number were incorporated in the macroscopic model. Since the interest in this paper is to investigate the overall performance of the macroscopic approach, we have not included any variation of properties here.

The average hot wall Nusselt number distribution with respect to the Rayleigh number is shown in Figure 6 for all the three cases considered. As seen, both the microscopic and macroscopic approach values are plotted in the same graph. Also the macroscopic results from the literature are included in the figure. The agreement between the two approaches is excellent for the first case, at the Darcy number of $8.98 \times 10^{-2}$ which is the highest of all the cases considered. However, at smaller Darcy numbers disagreements between the results are noticed, especially at higher Rayleigh numbers. This may be due to

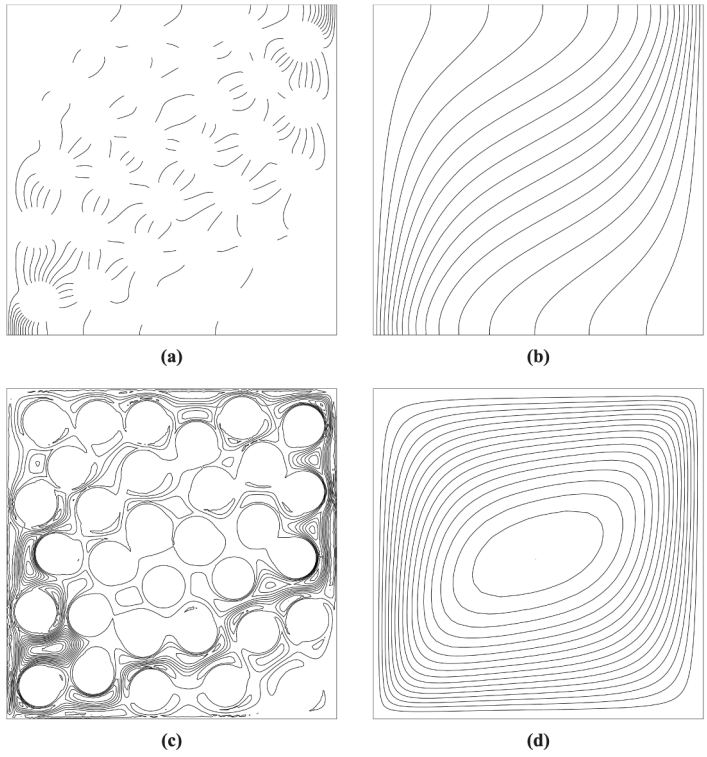


**Figure 5.**
Macroscopic (right) and microscopic (left) solutions. Isotherms (a, b) and streamlines (c, d) at $Ra = 10^4$ for the third case considered (macroscopic parameters: $\varepsilon = 0.607$, $Da = 9.68 \times 10^{-3}$)

two reasons. The first reason is that at lower Darcy numbers it is difficult to represent several activities of the microscopic approach using an averaged macroscopic model. The second reason is that at higher Rayleigh numbers, the validity of the two dimensional analysis may have limitations as noticed by others (Nakayama and Kuwahara, 2000). The results in terms of the average Nusselt number are also compared in Figure 6 with some of the results available in the literature (Lauriat and Prasad, 1989; Nithiarasu *et al.*, 1997). However, the available literature lacks in results related to the porous cavity saturated with air. Therefore, the last case (Figure 6(c)) was the only one that had the same macroscopic values close to the present cases. It should be noted here that a small deviation between the present results and those available in literature exist. This is mainly due to the difference in the Darcy and Prandtl numbers used between the literature and the present study. In the present study, the Prandtl number is assumed to be equal to 0.72 and the literature results are for a value of 1.0. Since there are no results found in the literature for the Darcy numbers used in the present study, the nearest Darcy number solution from literature is used for comparison.

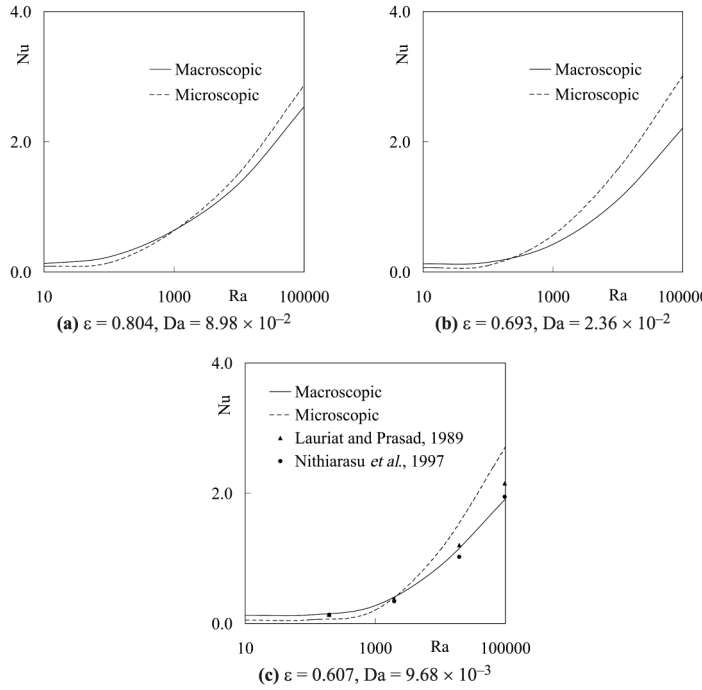


**Figure 6.**
Comparison of the average Nusselt number on the vertical walls, calculated for the macroscopic (continuous line) and microscopic (dashed line) solution for the different cases considered

*4.2 Porous medium – free fluid interface problems*

The problem of an interface between the porous media and free moving fluids is very interesting because of its implications in many real life problems. However, the problem has not been completely clarified yet. Microscopic solution can certainly help to get further insight into this complicated problem.

The computational domains considered for the microscopic and macroscopic solution of an interface problem are presented in Figure 7. A cavity with an aspect ratio of 0.5 is equally divided into two parts, one filled by a saturated porous medium and the other by the free fluid. The boundary conditions, equal for both cases, are similar to the porous medium problem presented in the previous subsection, and are presented in Figure 7. No-slip conditions are applied on all walls, horizontal walls are assumed to be insulated, and vertical walls are kept at different temperatures. Again the solid particles of the porous medium are considered to be adiabatic in the microscopic configuration, in order to reproduce the assumption of local thermal equilibrium made for the macroscopic approach.

In order to solve macroscopically the problem of interface between a porous medium and a free fluid, a suitable set of matching conditions is needed to connect the porous and single-phase domains. In the following section, these interface conditions are discussed in detail.

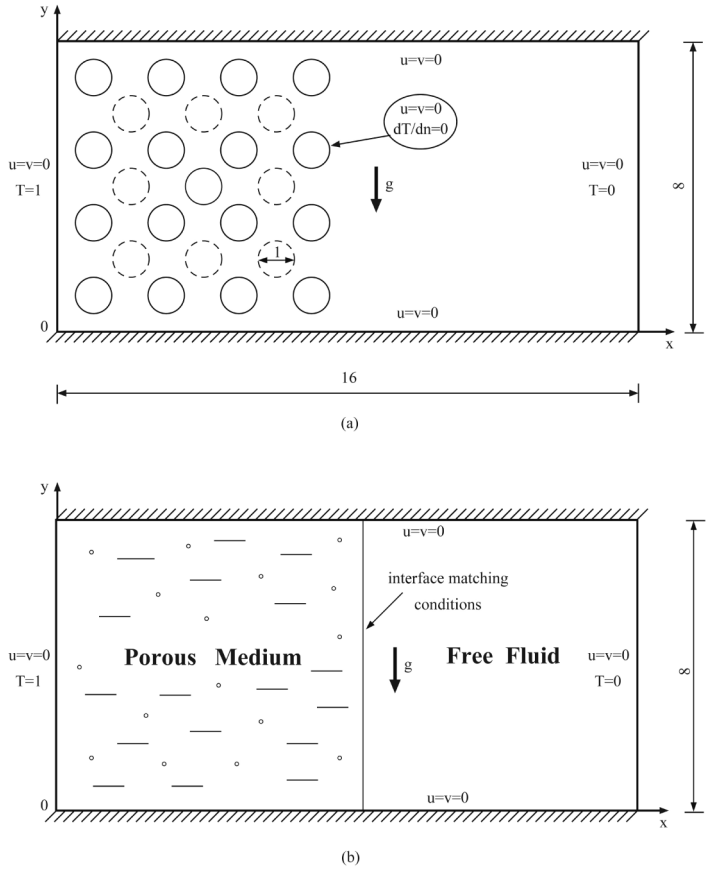


**Figure 7.**
Computational domain and boundary conditions used for the macroscopic (bottom) and the microscopic (top) approaches to the interface problem

*4.2.1 Interface matching conditions*. Matching conditions for velocity, pressure and temperature at interface between a porous layer and a free fluid are still not well established. Although mass, momentum and energy conservation clearly must be satisfied across the interface in the microscopic approach, there are still issues about what these conditions should become at the macroscopic level (Alazmi and Vafai, 2001; Kaviany, 1991; Nield and Bejan, 1992; Nield *et al.*, 1995). In the present work, no attempt has been made to establish any new conditions across the boundary and the classical continuity conditions have been employed.

When continuity of mass, momentum and energy is assumed, the following matching conditions need to be satisfied at the interface:

$$(u_i^{\mathrm{f}} - u_i^{\mathrm{p}})\, n_i = 0, \qquad (\sigma_{ij}^{\mathrm{f}} - \sigma_{ij}^{\mathrm{p}}) n_j = 0, \qquad (\tau_{ij}^{\mathrm{f}} - \tau_{ij}^{\mathrm{p}}) t_j = 0 \qquad (19)$$

where superscripts f and p refer, respectively, to the free fluid and porous medium; $n_i$ is the unit vector normal to the interface and $t_j$ is the unit vector in tangential direction; $\tau_{ij}$ is the deviatoric or viscous stress, and $\sigma_{ij}$ is the normal stress.

The above conservation equation, using the standard Newtonian constitutive relations for the tangential stress, do not provide any constrains on the tangential component of the velocity. This assumption is explicitly made in the present work.

Pressure is generally assumed to be continuous across the interface and this involves (equation (16)) that the normal components of the fluid viscous stress are balanced across the interface (Gartling *et al.*, 1996). Nield (1991) argued that in this way the stress in the solid matrix is not taken into account properly. The authors are aware of the fact that this assumption will lead to a slight over prediction of the flow magnitude and influx into the porous medium. However, this shortcoming may be overcome through a better understanding of the Brinkman viscosity, which is beyond the scope of this work. In this study the effective viscosity is assumed to be equal to the fluid viscosity. Further study on the calculation of equivalent viscosity is being carried out by the authors in order to get a better approximation of interface conditions.

With regards to thermal conditions, local thermal equilibrium and energy conservation are assumed along the interface, therefore the temperature and heat fluxes are considered to be continuous across the interface:

$$T^{\mathrm{f}} - T^{\mathrm{p}} = 0, \qquad \left(\frac{\partial T^{\mathrm{f}}}{\partial x_i} - R_{\mathrm{k}}\frac{\partial T^{\mathrm{p}}}{\partial x_{\mathrm{i}}}\right) n_i = 0 \tag{20}$$

With the above assumptions, the nodal equations (13)-(16) do not need any particular treatment at the interface. The nodes placed along the interface will get adequate contributions from elements placed in the fluid and in the porous medium.

*4.2.2 Interface results*. The mesh sensitivity analysis carried out for the interface problem has shown that about 10,000 nodes are necessary to obtain a mesh independent solution for the microscopic approach. For the macroscopic approach, a structured mesh of 4,000 nodes was found to be adequate.

The results obtained for the interface problem are presented in Figures 8-11 in terms of isotherms and stream functions for two of the three cases considered. Figure 8 presents the isotherms for the first case of 16 cylinders arranged in-line to microscopically describe the porous medium (left), and this figure also shows the corresponding macroscopic solutions (right). This again corresponds to a porous medium of porosity 0.804 and Darcy number of $8.98 \times 10^{-2}$. It can be noticed that the microscopic problem is very well reproduced qualitatively by the macroscopic solution for the Rayleigh number range considered.

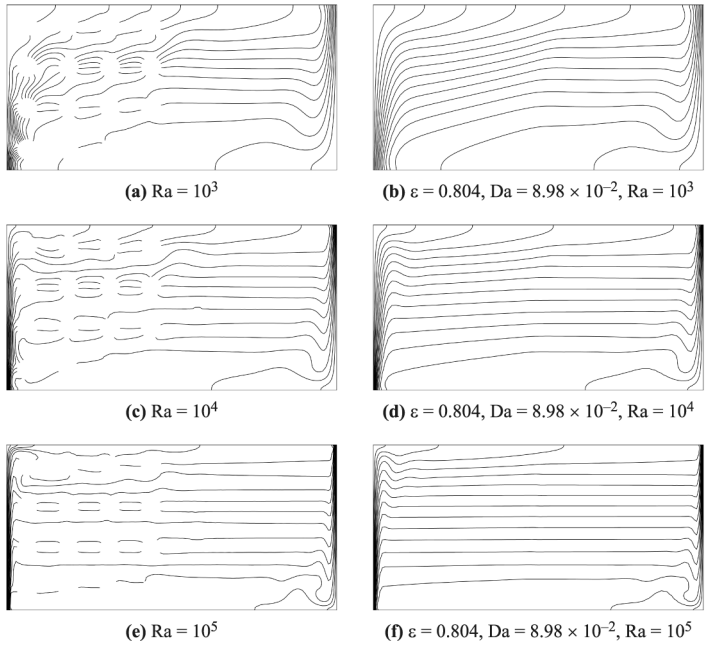

**(a)** Ra = $10^3$ **(b)** ε = 0.804, Da = 8.98 × $10^{-2}$, Ra = $10^3$

**(c)** Ra = $10^4$ **(d)** ε = 0.804, Da = 8.98 × $10^{-2}$, Ra = $10^4$

**(e)** Ra = $10^5$ **(f)** ε = 0.804, Da = 8.98 × $10^{-2}$, Ra = $10^5$

**Figure 8.**
Macroscopic (right) and microscopic (left) solution. Isotherms at different Rayleigh numbers for the in-line cylinder arrangement

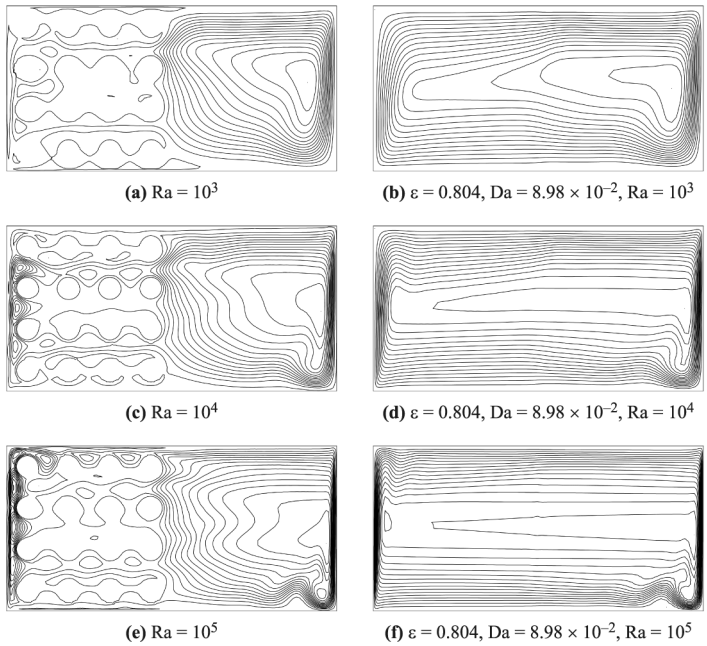

**(a)** Ra = $10^3$ **(b)** ε = 0.804, Da = 8.98 × $10^{-2}$, Ra = $10^3$

**(c)** Ra = $10^4$ **(d)** ε = 0.804, Da = 8.98 × $10^{-2}$, Ra = $10^4$

**(e)** Ra = $10^5$ **(f)** ε = 0.804, Da = 8.98 × $10^{-2}$, Ra = $10^5$

**Figure 9.**
Macroscopic (right) and microscopic (right) solution. Streamlines at different Rayleigh numbers for the in-line cylinder arrangement

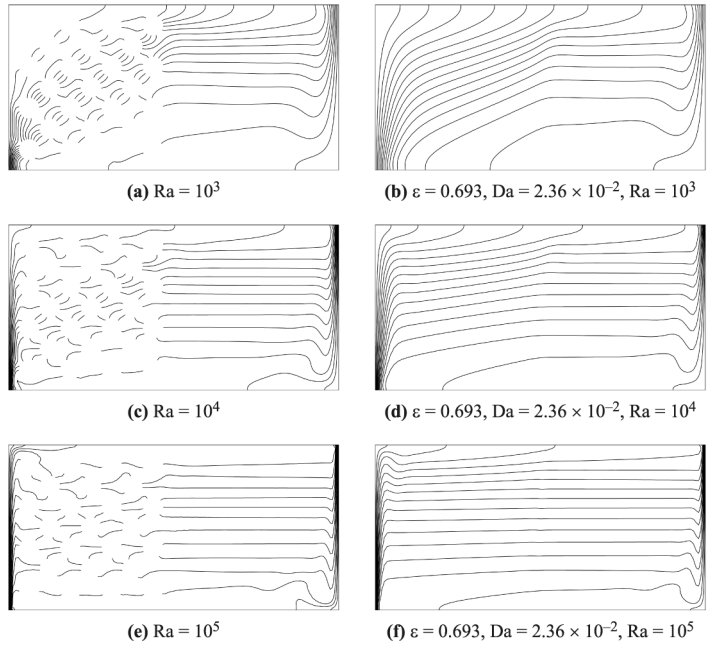


**Figure 10.**
Macroscopic (right) and microscopic (left) solutions. Isotherms at different Rayleigh numbers. Staggered cylinder arrangements

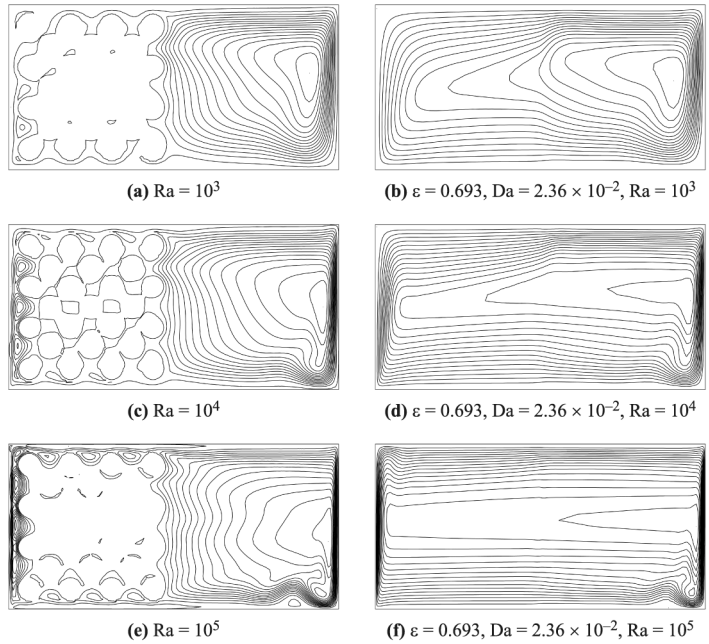


**Figure 11.**
Macroscopic (right) and microscopic (right) solutions. Isotherms at different Rayleigh numbers. Staggered cylinder arrangements

In fact, it is noted that a similarity exists between the streamlines of the microscopic and the macroscopic approaches as shown in Figure 9. In fact, in both approaches the eye of the vortex is placed in the free fluid part of the cavity, in a similar position. In the porous part, it can be noticed that in both approaches the streamlines become denser near the hot wall. However, the quantities to be compared in this part of the cavity have to be averaged, and cannot be seen to have the same trend.

The second case considered, similar to the one presented in the last subsection, is a porous medium with a different permeability. A staggered arrangement of 25 cylinders is employed in this case. The macroscopic properties of the porous medium, calculated from equation (3), for this case are: $\varepsilon = 0.693$ and $\kappa = 2.36 \times 10^{-2}$. The isotherms and the streamlines for this case are presented in Figures 10 and 11, respectively. It is seen that some discrepancies arise between the results obtained using the two approaches. This is clear from Figure 10, in which the isotherms in the fluid part of the cavity are seen to differ between the two approaches, especially at higher Rayleigh numbers.

However, the patterns obtained using the two approaches are still similar, as seen from the streamlines (Figure 11). Even here the difference between the two approaches widens as the Rayleigh number is increased (see Figure 11(e) and (f)).

The results for the last arrangement of particles considered is presented in Figures 12 and 13. The macroscopic properties of the porous medium are $\varepsilon = 0.607$ and $\kappa = 9.68 \times 10^{-3}$. The results obtained using the two approaches are again very similar, and tend to differ for higher values of the Rayleigh number. This can be noticed in particular from the streamlines presented in Figure 12.

Figure 14 shows the values of the average Nusselt number on the vertical walls obtained for the three porous medium – free fluid interface cases studied. These plots confirm what is expected from the results presented so far. At higher values of Darcy number and porosity the agreement between the microscopic and macroscopic approaches is excellent (Figure 14(a)). The comparison between the two approaches deteriorates as the Darcy number and the porosity reduce, except for the last case (Figure 14(c)). Although the average Nusselt number of the last case, with arbitrary cylinder arrangement, agrees excellently with the macroscopic Nusselt number, the difference between the two approaches is likely to increase further if Rayleigh number is increased. This is evident from the steep slope of the dotted line representing the microscopic approach in Figure 14(c).

In Figure 15, the values of the maximum absolute stream function $|\Phi|_{max}$ are presented for the different cases considered, as the Rayleigh number varies. In terms of this parameter the agreement between the two approaches can be seen to be even more pronounced than the heat transfer quantities. However, the

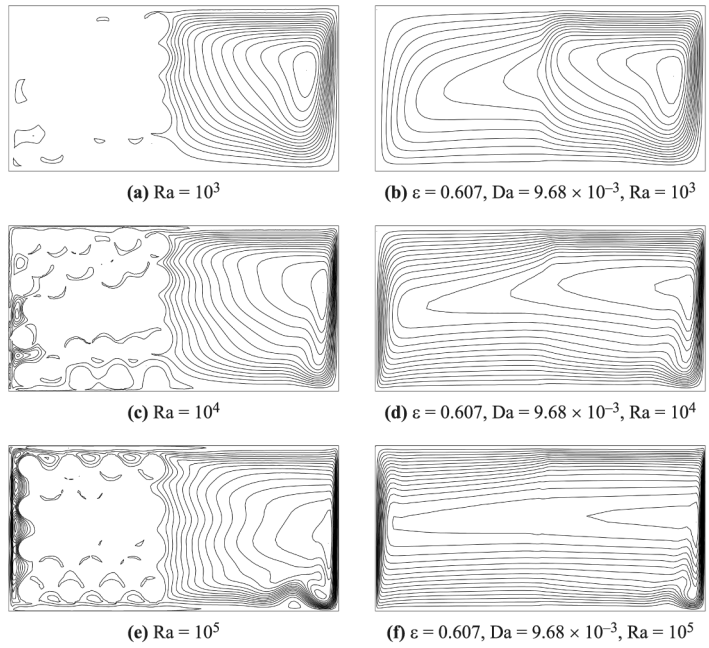


**Figure 12.**
Macroscopic (right) and microscopic (right) solutions. Isotherms at different Rayleigh numbers. Staggered cylinder arrangements

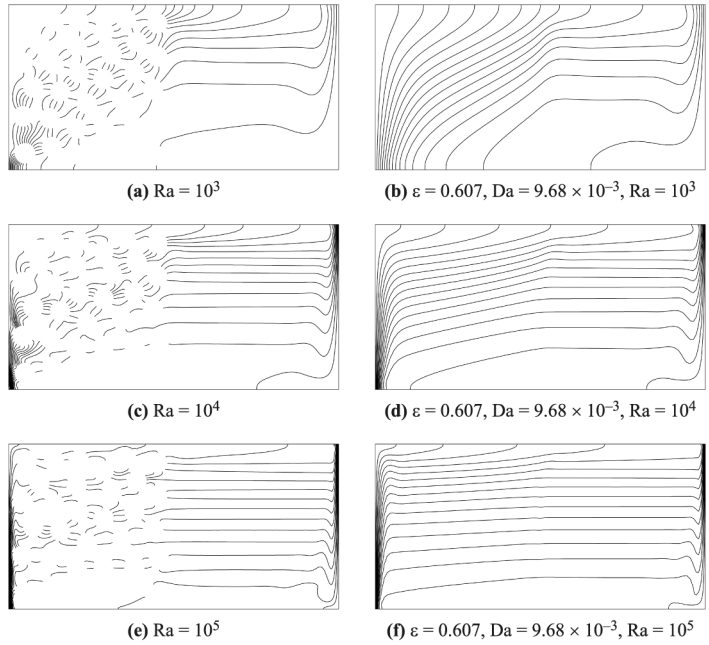


**Figure 13.**
Macroscopic (right) and microscopic (left) solutions. Isotherms at different Rayleigh numbers. Staggered cylinder arrangements

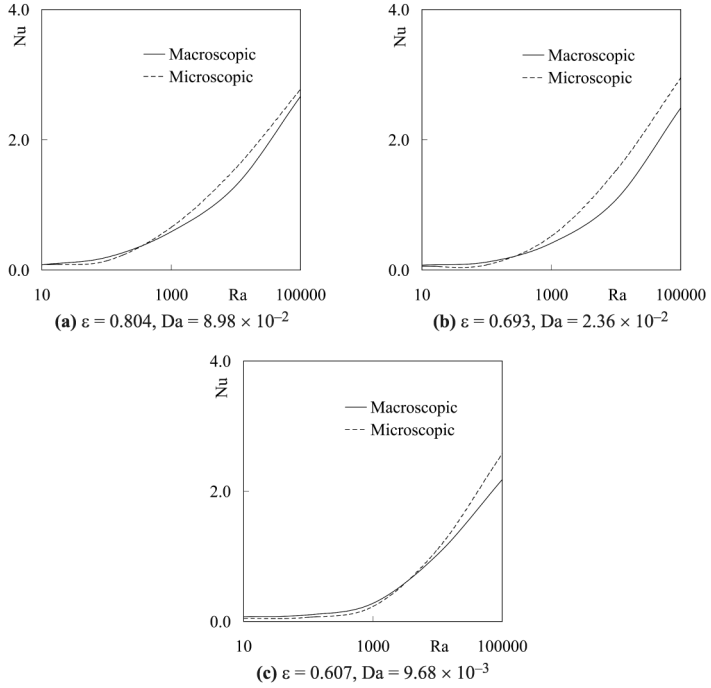


**Figure 14.**
Comparison of the average Nusselt number on the vertical walls calculated from the macroscopic (continuous line) and microscopic (dashed line) solutions for different interface configurations considered

figure confirms what was found before, the comparison deteriorates as the Darcy number and the porosity reduce.

## 5. Conclusions

In this paper, a numerical simulation of the natural convection in porous enclosures partly or fully occupied by a saturated porous medium has been carried out. Problems are solved using both the microscopic and the macroscopic approaches, in order to evaluate the relations between these two approaches. Therefore, the porous medium is treated first as an array of solid cylindrical particles (microscopic approach), and then a generalised model is used for the description of the averaged porous medium flow (macroscopic approach). The CBS algorithm is employed in both approaches because of its well known performance in the solution of fluid dynamic problems.

For all the problems studied in this paper, an excellent agreement between the microscopic and macroscopic approaches has been noticed at high Darcy number and porosity. However, the results differ between these two approaches at lower Darcy number and porosity, especially at higher Rayleigh numbers. It should be noted that the agreement between the macroscopic and the macroscopic approaches may be improved by employing

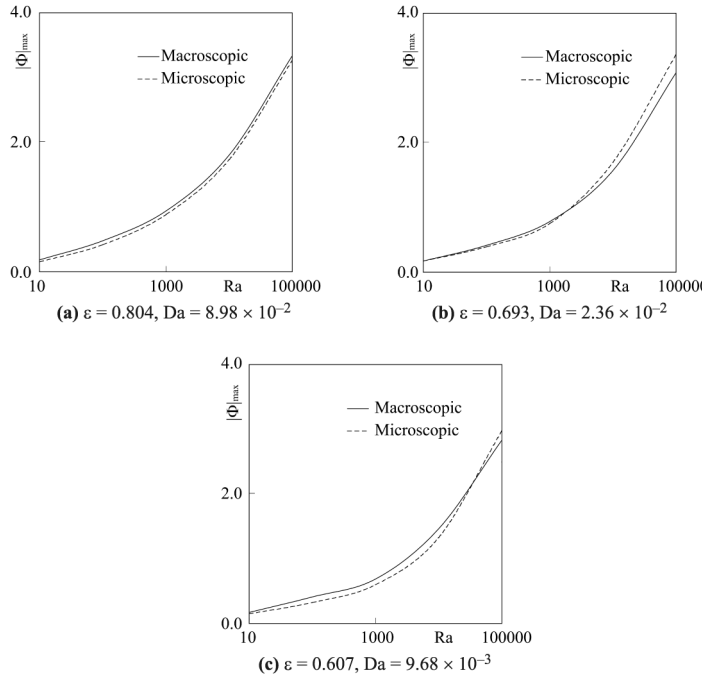


**Figure 15.**
Comparison of the maximum absolute value of the stream function $|\Phi|_{max}$ calculated from the macroscopic (continuous line) and microscopic (dashed line) solutions for different interface configurations considered

three dimensional analysis, as reported by Nakayama and Kuwahara (2000) in the context of forced flows. It is obvious that better definitions of permeability and porosity are possible in three dimension. The analysis in three dimensions is already well under way and expected to give further insight into the relations between the microscopic and the macroscopic approaches.

## References

Alazmi, B. and Vafai, K. (2001), "Analysis of fluid flow and heat transfer interfacial conditions between a porous medium and a fluid layer", *Int. J. Heat Mass Transfer*, Vol. 44, pp. 1735-49.

Beckermann, C., Ramadhyani, S. and Viskanta, R. (1987), "Natural convection flow and heat transfer between a fluid layer and a porous layer inside a rectangular enclosure", *ASME J. Heat Transfer*, Vol. 109, pp. 363-70.

Brinkmann, H.C. (1947), "A calculation of the viscous force exerted by a flowing fluid on a dense swarm of particles", *Appl. Sci. Res.*, Vol. A1, pp. 27-34.

Brinkmann, H.C. (1948), "On the permeability of media consisting of closely packed porous particles", *Appl. Sci. Res.*, Vol. A1, pp. 81-6.

Darcy, H. (1856), *Les fontaines publiques de la ville de Dijon*, Dalmont, Paris.

Ergun, S. (1952), "Fluid flow through packed column", *Chem. Eng. Prog.*, Vol. 48, pp. 89-94.

Forchheimer, P. (1901), "Wasserbewegung durch bodem", *Z. Ver. Deutsch*, Vol. 45.

Fu, W.S. and Chen, S.F. (2002), "A numerical study of heat transfer of a porous block with the random porosity model in a channel flow", *Heat Mass Transfer*, Vol. 38, pp. 695-704.

Gartling, D.K., Hickox, C.E. and Givler, R.C. (1996), "Simulation of coupled viscous and porous flow problems", *Comp. Fluid Dyn.*, Vol. 7, pp. 23-48.

Gilver, R.C. and Altobelli, S.A. (1994), "A determination of the effective viscosity for the Brinkman-Forchhiemer flow model", *J. Fluid Mech.*, Vol. 258, pp. 355-70.

Gupte, S.K. and Advani, S.G. (1997), "Flow near the permeable boundary of a porous medium: an experimental investigation using LDA", *Exp. Fluids*, Vol. 22, pp. 408-22.

Heindel, T.J., Incropera, F.P. and Ramadhyami, S. (1996), "Enhancement of natural convection heat transfer from an array of discrete heat sources", *Int. J. Heat Mass Transfer*, Vol. 39, pp. 479-90.

Hsu, C.T. and Cheng, P. (1990), "Thermal dispersion in a porous medium", *Int. J. Heat Mass Transfer*, Vol. 33, pp. 1587-97.

Kaviany, M. (1991), *Principles of Heat Transfer in Porous Media*, Springer-Verlag, New York.

Kladias, N. and Prasad, V. (1991), "Experimental verification of Darcy-Brinkman-Forchheimer flow model for natural convection in porous media", *J. Thermophysics*, Vol. 5, pp. 560-76.

Koplik, J., Levine, H. and Zee, A. (1983), "Viscosity renormalization in the Brinkman equation", *Phys. Fluids*, Vol. 26, pp. 2864-70.

Lauriat, G. and Prasad, V. (1989), "Non-Darcy effects on natural convection in a vertical porous enclosure", *Int. J. Heat Mass Transfer*, Vol. 32, pp. 2135-48.

Lee, S.L. and Yang, J.H. (1997), "Modelling of Darcy-Forchheimer drag for fluid flow across a bank of circular cylinders", *Int. J. Heat Mass Transfer*, Vol. 40, pp. 3149-55.

Maji, P.K. and Biswas, G. (1999), "Analysis of flow in the spiral casing using a streamline upwind Petrov-Galerkin method", *Int. J. Num. Meth. Eng.*, Vol. 45, pp. 147-74.

Martys, N., Bentz, D.P. and Garboczi, E.J. (1994), "Computer simulation study of the effective viscosity in Brinkman's equation", *Phys. Fluids*, Vol. 6, pp. 1434-9.

Massarotti, N. (2001), "The characteristic-based-split algorithm for the solution of porous medium flow problems, PhD thesis, University of Wales Swansea, Wales, UK.

Massarotti, N., Nithiarasu, P. and Zienkiewicz, O.C. (1998), "Characteristic based-split (CBS) algorithm for incompressible flow problems with heat transfer", *Int. J. Num. Meth. Heat Fluid Flow*, Vol. 8, pp. 969-90.

Massarotti, N., Nithiarasu, P. and Zienkiewicz, O.C. (2000), "Porous-fluid interface problems, a characteristic-based-split (CBS) procedure", *Proceedings of the ECCOMAS 2000*, 11-14 September, Barcelona, Spain.

Massarotti, N., Nithiarasu, P. and Zienkiewicz, O.C. (2001), "Natural convection in porous medium – free fluid interface problems, a finite element analysis by using the CBS procedure", *Int. J. Num. Meth. Heat Fluid Flow*, Vol. 11, pp. 473-90.

Nakayama, A. and Kuwahara, F. (2000), "Numerical modeling using microscopic structures", in Vafai, K. (Ed.), *Handbook of Porous Media*, Chapter 10, Marcel Dekker, New York.

Nield, D.A. (1991), "The limitations of the Brinkmann-Forchheimer equation in modeling flow in a saturated porous medium and at an interface", *Int. J. Heat Fluid Flow*, Vol. 12, pp. 269-72.

Nield, D.A. and Bejan, A. (1992), *Convection in Porous Media*, Springer-Verlag, New York.

Nield, D.A., Vafai, K. and Kim, S.J. (1995), "Closure statements on the Brinkman-Forchheimer-extended Dracy model", *Int. J. Heat Fluid Flow*, Vol. 17, pp. 34-5.

Nithiarasu, P. (1999), "Finite element modelling of migration of a third component leakage from a heat source buried into a fluid saturated porous medium", *Mathematical and Computer Modelling*, Vol. 29, pp. 27-39.

Nithiarasu, P. and Ravindran, K. (1998), "A new semi-implicit time stepping procedure for buoyancy driven flow in saturated porous medium", *Comp. Meth. Appl. Mech. Eng.*, Vol. 165, pp. 147-54.

Nithiarasu, P., Seetharamu, K.N. and Sundararajan, T. (1996), "Double-diffusive natural convection in an enclosure filled with saturated porous medium a generalized non-Darcy approach", *Num. Heat Transfer, Part A*, Vol. 30, pp. 413-26.

Nithiarasu, P., Seetharamu, K.N. and Sundararajan, T. (1997), "Natural convective heat transfer in an enclosure filled with fluid saturated variable porosity medium", *Int. J. Heat Mass Transfer*, Vol. 40, pp. 3955-67.

Nithiarasu, P., Seetharamu, K.N. and Sundararajan, T. (1998a), "Finite element analysis of pollutant transport in water saturated soil", *Comm. Num. Meth. Eng.*, Vol. 14, pp. 241-51.

Nithiarasu, P., Seetharamu, K.N. and Sundararajan, T. (1998b), "Effects of porosity on natural convective heat transfer in a fluid saturated porous medium", *International Journal of Heat and Fluid flow*, Vol. 19, pp. 56-8.

Nithiarasu, P., Seetharamu, K.N. and Sundararajan, T. (2002), "Finite element modeling of flow heat and mass transfer in fluid saturated porous media", *Arch. Mech.*, Vol. 9, pp. 3-42.

Nithiarasu, P., Sujatha, K.S., Ravindran, K., Seetharamu, K.N. and Sundararajan, T. (2000), "Non-Darcy natural convection in a hydrodynamically and thermally anisotropic porous medium", *Comp. Meth. Appl. Mech. Eng.*, Vol. 188, pp. 413-30.

Oosthuizen, P.H. (2000), "Natural convective heat transfer in porous-media-filled enclosures", in Vafai, K. (Ed.), *Handbook of Porous Media*, Chapter 11, Marcel Dekker, New York.

Prescott, P.J. and Incropera, F.P. (1994), "Convective transport phenomena and macrosegregation during solidification of a binary metal alloy: I – Numerical predictions", *ASME J. Heat Transfer*, Vol. 116, pp. 735-41.

Song, M. and Viskanta, R. (1994), "Natural convection flow and heat transfer within a rectangular enclosure containing a vertical porous layer", *Int. J. Heat Transfer*, Vol. 37, pp. 2425-38.

Tong, T.W. and Subramanian, E. (1986), "Natural convection in rectangular enclosures partially filled with a porous medium", *Int. J. Heat Fluid Flow*, Vol. 7, pp. 3-10.

Vafai, K. and Tien, C.L. (1981), "Boundary and inertia effects on flow and heat transfer in porous media", *Int. J. Heat Mass Transfer*, Vol. 24, pp. 195-203.

Wang, C.Y. (1999), "Longitudinal flow past cylinders arranged in a triangular array", *Appl. Math. Mod.*, Vol. 23, pp. 219-30.

Whitaker, S. (1961), "Diffusion and dispersion in porous media", *AIChE J.*, Vol. 13, pp. 420-7.

Zhao, C.Y. and Lu, T.J. (2002), "Analysis of microchannel heat sinks for electronic cooling", *Int. J. Heat Mass Transfer*, Vol. 45, pp. 4857-69.

Zienkiewicz, O.C. and Taylor, R.L. (2000), "The finite element method", *Fluid Dynamics*, Arnold, London, UK, Vol. 3, p. 1.